Transient, sparsely-populated compact states of apo and calcium-loaded calmodulin probed by paramagnetic relaxation enhancement: interplay of conformational selection and induced fit

Nicholas J. Anthis, **Michaeleen Doucleff**[1], and **G. Marius Clore**[*]
Laboratory of Chemical Physics, National Institute of Diabetes and Digestive and Kidney Diseases, National Institutes of Health, Bethesda, Maryland 20892-0520, U.S.A

Abstract

Calmodulin (CaM) is the universal calcium sensor in eukaryotes, regulating the function of numerous proteins. Crystallography and NMR show that free CaM-4Ca^{2+} exists in an extended conformation with significant interdomain separation, but clamps down upon target peptides to form a highly compact structure. NMR has revealed substantial interdomain motions in CaM-4Ca^{2+}, enabled by a flexible linker. In one instance, CaM-4Ca^{2+} has been crystallized in a compact configuration; however, no direct evidence for transient interdomain contacts has been observed in solution, and little is known about how large-scale interdomain motions contribute to biological function. Here we use paramagnetic relaxation enhancement (PRE) to characterize transient compact states of free CaM that are too sparsely populated to observe by traditional NMR methods. We show that unbound CaM samples a range of compact structures, populated at 5–10%, and that Ca^{2+} dramatically alters the distribution of these configurations in favor of states resembling the peptide-bound structure. In the absence of Ca^{2+}, the target peptide binds only to the C-terminal domain, and the distribution of compact states is similar with and without peptide. These data suggest an alternative pathway of CaM action in which CaM remains associated with its kinase targets even in the resting state. Only CaM-4Ca^{2+}, however, shows an innate propensity to form the physiologically active compact structures, suggesting that Ca^{2+} activates CaM not only through local structural changes within each domain but also through more global remodeling of interdomain interactions. Thus, these findings illustrate the subtle interplay between conformational selection and induced fit.

Introduction

As the cell's prototypical Ca^{2+} sensor, calmodulin (CaM) is responsible for amplifying and adapting this universal signal into specific downstream signals via interactions with hundreds of other proteins. This biological adaptability correlates with the significant structural plasticity that has been observed in CaM.[1] Fig. 1 summarizes existing static structures of apo CaM,[2] CaM-4Ca^{2+},[3] and the complex between CaM-4Ca^{2+} and the CaM binding domain (CBD) of myosin light chain kinase (MLCK),[4] Upon binding calcium, 25–50° shifts in the interhelical angles within the two domains of CaM expose methionine-rich hydrophobic patches,[2,5] thereby priming CaM to interact with a variety of binding partners

that are self-inhibited by a CBD in the resting state (such as MLCK and other kinases). Target self-inhibition is relieved upon binding of CaM-4Ca^{2+} to form a highly compact structure (CaM-4Ca^{2+}-MLCK) in which the N- and C-terminal domains of CaM are clamped around an α-helical CBD peptide and make contact with one another.[4,6] This is accomplished primarily through extensive bending of the central linker, with the two domains of CaM behaving largely as rigid bodies, and through the concerted formation of an extensive network of hydrophobic and ion-pair interactions between the helical peptide and the two domains of CaM.[7] Although CaM can also form other types of complexes, with differing Ca^{2+} dependencies,[1,8] we concern ourselves here specifically with the canonical Ca^{2+}-dependent 1:1 CaM:peptide interaction, represented by CaM-4Ca^{2+}-MLCK (Fig. 1*C*).

Although all crystal structures of free CaM-4Ca^{2+} (e.g. refs 3,9,10), with one exception,[11] appear as an extended dumbbell structure with a contiguous central helix connecting the two domains separated by a center-to-center distance of ~40 Å (Fig. 1*B*), fluorescence energy transfer experiments[12] and small angle X-ray and neutron scattering[13] indicate that the average structure of CaM-4Ca^{2+} in solution is somewhat more compact. NMR relaxation studies on both apo CaM[14] and CaM-4Ca^{2+} [15,16] have shown unambiguously that the central residues (77-81) of the linker are highly mobile (with S^2 order parameters of 0.5–0.6), and that the two domains reorient almost independently of one another in solution on a time scale of ~3 ns, undergoing restricted diffusion within a cone of semi-angle ~30°. Studies based on lanthanide-induced residual dipolar couplings (RDC) and pseudo-contact shifts (PCS) suggest that an even larger cone of semi-angle 50–80° can be sampled.[17] In one instance, CaM-4Ca^{2+} has been crystallized in a compact conformation that resembles the peptide-bound structure,[11] but this specific conformation must have been largely selected by crystal packing forces since there is no conventional NMR evidence (in the form of interdomain nuclear Overhauser effects (NOE)) for any direct contacts between the N- and C-terminal domains of CaM-4Ca^{2+}.[18] Thus the population of such a state, if it exists, must be very low in solution. Ensemble molecular dynamics (MD) simulations[19] also suggest that compact states can potentially be sampled, but it is unclear whether the empirical force field employed is sufficiently accurate or the sampling sufficiently extensive to reliably characterize such states.

Our goal in the current work is to directly probe and visualize compact, sparsely-populated conformational substates of CaM, characterized by interdomain contacts, using paramagnetic relaxation enhancement (PRE), to determine how these differ in the presence and absence of Ca^{2+}, and how such states may contribute to CaM function. These sparsely-populated states are invisible to conventional structural biology techniques, owing to their low occupancy and transient nature. In the fast exchange regime, however, the footprint of sparsely-populated states can be observed on the PRE profile of the major species, provided that the distances between the paramagnetic label and the protons of interest are shorter in the minor species than the major one.[20] The exquisite sensitivity of the PRE in this regard arises from the large magnetic moment of the unpaired electron and the $<r^{-6}>$ dependence of the transverse PRE rate (Γ_2), resulting in extremely large Γ_2 values at short distances.[21] Since interdomain motion in CaM takes place on the nanosecond time scale,[14–16] any CaM conformations exhibiting close interdomain contacts should be observable by PRE, thereby offering novel insights over prior studies, which, by their nature, primarily characterized the major, more extended states of CaM-4Ca^{2+}.

Materials and Methods

Mutagenesis, and protein expression

The 148-residue calmodulin (CaM) protein from *Xenopus laevis* (identical in amino acid sequence to human CaM) was cloned into the pET21a (Novagen) vector using PCR primers

with *BamH1* and *NdeI* restriction sites. Spin-label sites were created by making single cysteine point mutations (T5C, S17C, T117C, and A128C) with the QuikChange Site-Directed Mutagenesis Kit (Stratagene).

Uniformly ^{2}H/^{13}C/^{15}N-labeled CaM was expressed in BL21-CodonPlus (DE3) RIPL cells (Stratagene) at 37°C using standard methods. Briefly, cells were grown in 1 L of M9 medium (using ^{2}H$_2$O, ^{15}NH$_4$Cl and [^{2}H$_7$,^{13}C$_6$]-glucose as isotope sources) and induced with 1 mM isopropyl β-D-1-thiogalactopyranoside (IPTG) at A$_{600nm}$ ~ 0.6. Cells were harvested by centrifugation 6–9 hours later.

Protein purification and nitroxide spin-labeling

Cells were resuspended in 40 mM Tris, pH 7.4, 2 mM ethylenediaminetetraacetic acid (EDTA), 2 mM dithiothreitol (DTT), and 1× Roche Complete Protease Inhibitor. Cells were lysed using a microfluidizer, cleared by centrifugation, and then loaded on a DEAE ion-exchange column (GE Life Sciences) pre-equilibrated with 20 mM Tris, pH 7.4, 80 mM (NH$_4$)$_2$SO$_4$ and 1 mM MgCl$_2$. Protein was eluted with a 0–100% gradient over 10 column volumes with a high-salt buffer containing 1.2 M (NH$_4$)$_2$SO$_4$. Relevant fractions were pooled and loaded onto phenyl-sepharose resin (GE Life Sciences) pre-equilibrated with 50 mM Tris, pH 7.4, 2 mM CaCl$_2$ and 100 mM NaCl. CaM was eluted with the addition of 2 mM ethylene glycol tetraacetic acid (EGTA). Protein was stored in the elution buffer plus 0.5 mM tris(2-carboxyethyl)phosphine (TCEP) and 1× Roche Complete Protease Inhibitor.

CaM was paramagnetically labeled by the addition of a 10-fold excess of the nitroxide spin-label (1-Oxyl-2,2,5,5-tetramethyl-δ-3-pyrroline-3-methyl) methanethiosulfonate ("MTSL"; Toronto Research Chemicals) to ~200 μM CaM. The reaction was allowed to proceed in the dark for 2 hours and tested for completion by mass spectroscopy. The diamagnetic control was labeled by the same method using (1-Acetoxy-2,2,5,5-tetramethyl-δ-3-pyrroline-3-methyl) methanethiosulfonate (Toronto Research Chemicals).

Unreacted spin-label was removed with a HiPrep 26/10 Desalting Column (GE Life Sciences) and exchanged into NMR buffer, comprising 5% D$_2$O/95% H$_2$O, 100 mM KCl, 0.1× Roche Complete Protease Inhibitor, 25 mM HEPES, pH 6.5, and either 8 mM CaCl$_2$ (for Ca^{2+}- bound CaM) or 2 mM EDTA and 2 mM EGTA (for apo CaM). NMR samples were concentrated to 0.3 mM with Amicon Ultra Centrifugal Filter Units (3 kDa molecular weight cutoff). For isothermal titration calorimetry (ITC), NMR assignment experiments, or other work on wild type protein, CaM was purified as above, except instead of spin-labeling, buffer exchange was performed immediately following phenyl-sepharose purification. Experiments were performed on CaM alone, or in the presence of a synthetic peptide (KRRWKKNFIAVSAANRFKKISSSG AL; Anaspec), corresponding to the CaM-binding domain (CBD) of human skeletal muscle myosin light chain kinase (skMLCK). For Ca^{2+}-loaded CaM, a 1.2-fold excess of peptide was added, and the sample was then concentrated to 0.3 mM CaM. For apo CaM, final NMR samples were made directly with 0.3 mM CaM and a 2-fold excess of peptide.

Isothermal titration calorimetry

ITC was performed on a MicroCal iTC$_{200}$ calorimeter with CaM in the instrument cell and MLCK peptide in the injection syringe. Experiments were carried out at 27°C in NMR buffer. Sixteen 2.4-μL injections were performed (5 seconds each, separated by 180-second intervals). Experimental data were analyzed using MicroCal Origin software.

NMR Spectroscopy

NMR experiments were performed on uniformly ^{2}H/^{13}C/^{15}N-labeled CaM. Backbone resonance assignments for apo CaM, CaM-4Ca^{2+}, and CaM-4Ca^{2+}-MLCK were obtained by triple resonance through-bond scalar correlation spectroscopy[22] using HNCO, HNCACB, and CBCA(CO)NH pulse sequences. Data were processed using NMRPipe[23] and analyzed with the program XIPP (in-house software written by D.S. Garrett). Transverse ^{1}H$_N$-Γ_2 PRE rates were obtained from the differences in the transverse ^{1}H$_N$-R_2 relaxation rates between the paramagnetic and diamagnetic samples[21] using either of two different pulse sequences, which yielded identical results within experimental error. Some measurements used a 3D HNCO-based pulse scheme similar to that described by Hu et al.,[24] but without using transverse relaxation optimized spectroscopy (TROSY). Others used a TROSY version of a 2D pulse scheme similar to that depicted by Iwahara et al.,[25] but with the variable delay performed at the end of the pulse sequence, thus measuring the TROSY ^{1}H$_N$-R_2. Data were recorded at 27°C on a Bruker 600 MHz spectrometer equipped with a triple resonance z-gradient cryoprobe. Two time points (separated by 20 ms) were used for the ^{1}H$_N$-R_2 measurements, and the errors in the ^{1}H$_N$-Γ_2 PRE rates were calculated as described previously.[25] Samples for PRE experiments contained 0.3 mM ^{2}H/^{13}C/^{15}N-labeled spin-labeled (or control) CaM. Control experiments were also performed to detect any intermolecular PREs that might be present. In these cases, measurements were made on 0.3 mM ^{2}H/^{13}C/^{15}N-labeled CaM with no spin label in the presence of 0.3 mM CaM at natural isotopic abundance (either spin-labeled or wild type for diamagnetic control).

^{1}H-^{15}N heteronuclear single quantum coherence (HSQC) correlation spectroscopy was used to follow the ^{1}H$_N$/^{15}N chemical shifts of ^{15}N-labeled CaM (0.1 mM) upon addition of increasing amounts of unlabeled MLCK peptide. Weighted combined ^{1}H$_N$ and ^{15}N amide shifts, $\Delta(H_N,N)$, for CaM saturated with MLCK peptide were calculated using the equation:

$$\Delta(H_N, N) = \sqrt{(\Delta_H W_H)^2 + (\Delta_N W_N)^2}$$ where W_H and W_N are weighting factors for the ^{1}H and ^{15}N amide shifts, respectively ($W_H = 1$, $W_N = 0.154$, based on average variances [26] in the BioMagResBank; http://www.bmrb.wisc.edu[27]), and Δ is the chemical shift difference between bound and free states, $\delta_{bound} - \delta_{free}$.

PRE back-calculations and ensemble simulated annealing

Theoretical ^{1}H$_N$-Γ_2 PREs were back-calculated for each nitroxide spin-label position from the coordinates of the structure of CaM in four different states: (i) the Ca^{2+}-loaded extended "dumbbell" configuration (PDB 1CLL),[3] (ii) the Ca^{2+}-loaded, peptide-bound complex with smooth muscle MLCK (PDB 1CDL),[4] (iii) apo CaM (PDB 1CFD),[2] and (iv) the Ca^{2+}-loaded (peptide free) compact configuration of CaM (PDB 1PRW).[11] All of these structures are X-ray structures, with one exception, apo CaM (1CFD), which was solved by NMR. ^{1}H$_N$-Γ_2 rates were back-calculated in Xplor-NIH[28,29] using a five-conformer ensemble for the spin-label together with the Solomon-Bloembergen Model Free (SBMF) representation, optimizing the coordinate positions in torsion angle space by simulated annealing to minimize the difference between observed and calculated ^{1}H$_N$-Γ_2 PRE rates, as described previously.[30] In addition to the PRE pseudo-potential, the target function includes stereochemical restraints, a quartic van der Waals repulsion term to prevent atomic overlap between the spin-label and the protein, and a multidimensional torsion angle database potential of mean force.[31] (Note atomic overlap between spin-label ensemble members is allowed since the ensemble represents a distribution of states). For the spin-labels at positions S17C and A128C, the entire molecule, with the exception of side chains adjacent to the spin-label (which were given torsional degrees of freedom), was kept rigid during the fitting procedure. For the spin-labels at positions T5C and T117C, residues 1-8 and 115-120, respectively, were also given torsional degrees of freedom and represented by the same five-

member ensemble as the spin-label itself, to account for local structural perturbations induced by the spin-label (Fig. S3). Unless stated otherwise, spin-label positions were set by fitting to intradomain PRE data only.

Because the electron relaxation rate τ_s of the nitroxide spin-label is much longer than that of the protein rotational correlation time τ_r,[25] the PRE correlation time τ_c $[=(\tau_r^{-1} + \tau_s^{-1})^{-1}]$ for the calculation of PRE rates was assumed to be approximately the same as τ_r (9.9 ns) for CaM-$4Ca^{2+}$,[32] Agreement between observed and calculated Γ_2 rates is given by the PRE Q-factor:[30]

$$Q=\left[\sum_i \left\{ \Gamma_{2,i}^{obs} - \left\langle \Gamma_{2,i}^{calc} \right\rangle \right\}^2 \Big/ \sum_i \left(\Gamma_{2,i}^{obs} \right)^2 \right]^{1/2}$$

(1)

where $\Gamma_{2,i}^{obs}$ and $\left\langle \Gamma_{2,i}^{calc} \right\rangle$ are the observed and ensemble average back-calculated transverse Γ_2 rates for residue i, respectively. All members of the ensemble are weighted equally.

To optimize agreement with the interdomain PREs for all specified spin-labels simultaneously, ensembles of minor states were calculated using the ensembleSimulation module in Xplor-NIH.[33] Spin-label positions (represented by a five-member ensemble) were first set by fitting the intradomain PREs as described above. Conjoined rigid body/torsion angle simulated annealing[34] was then performed using an ensemble of minor states (consisting of 0 to 16 members and making up 0–40% of the total population): the two domains of CaM were treated as rigid bodies, and only the interdomain linker region (residues 77-81) was given torsional degrees of freedom. The target function was the same as that used to fit the intradomain PREs. The radial and angular order parameters for the SBMF representation (that are calculated on the fly from the coordinates during simulated annealing) were computed separately for each ensemble member rather than averaged over the entire ensemble. This is because the time scale of motion of the spin-label (represented by a five-member configuration for every member of the minor state ensemble) is much faster (picosecond regime) and therefore decoupled from the slower interdomain reorientations (nanosecond regime).

Each simulated annealing calculation was run 100 times, and the results were represented as reweighted atomic probability density maps.[35] Images of the probability maps and protein structures were generated using PyMOL (http://www.pymol.org).

Results and Discussion

CaM-Peptide Interactions, Spin Labeling, and PRE Measurements

Large backbone $^1H_N/^{15}N$ chemical shift perturbations throughout CaM-$4Ca^{2+}$ are observed upon binding the MLCK peptide, particularly in the central linker (Fig. 1*D*). Interestingly, we also detected binding of the MLCK peptide to apo CaM, albeit two order of magnitude weaker than in the presence of Ca^{2+} ($K_D \sim 1$ μM versus 10 nM; Supplementary Fig. S1). Exchange between free and peptide-bound states is fast on the chemical shift time scale for apo CaM but slow for CaM-$4Ca^{2+}$ (Supplementary Fig. S2). The peptide-induced chemical shift perturbations in apo CaM are much smaller in magnitude than those observed for CaM-$4Ca^{2+}$, and are restricted primarily to the C-terminal domain (Fig. 1*D*). That such an interaction is observed at all suggests that Ca^{2+}/CaM activation of MLCKs may be more complicated than the conventional mechanism illustrated in Figs. 1*A*–*C*. Thus, to explore this mechanism, and the role of interdomain dynamics, PREs were measured for Ca^{2+}-

loaded and Ca^{2+}-free CaM, in the presence and absence of the MLCK CBD peptide. Nitroxide spin-labels were conjugated via S-S linkages to engineered surface cysteines strategically placed at four positions: T5C, S17C, T117C, A128C (Figs. 1*A–C*, and Supplementary Fig. S3*B*). CaM-4Ca^{2+} displays wild type peptide binding activity for each spin-label (Supplementary Fig. S1). No evidence was observed for structural or dynamic effects induced by the spin-labels at S17C or A128C; however, labels at positions T5C and T117C result in local structural heterogeneity (Supplementary Fig. S3), likely due to a small degree of fraying at the N-terminal ends of helices I and VII, respectively, owing to disruption of an N-cap side chain-backbone hydrogen bond between the threonine hydroxyl oxygen atom and the backbone amide of the *i*+3 residue.[3] Although these effects are minor and can be accounted for (Supplementary Figs. S3 and S4), they complicate PRE analysis. Hence, this work relies primarily on the S17C and A128C data, while the T5C and T117C data are used only for independent validation purposes (see below).

Interdomain PREs are observed for CaM-4Ca^{2+} and apo CaM (with or without bound peptide), which differ both in terms of their profiles and magnitude, with the latter (Fig. 2, panels on lower two rows) being significantly smaller than the former (Fig. 2, panels on second row). Thus one can immediately conclude that sparsely-populated states of CaM-4Ca^{2+} and apo CaM, characterized by close interdomain contacts and undetected by NOEs, are sampled in solution and that the distribution of these states is modulated by calcium. In addition, PRE experiments were also performed on CaM-4Ca^{2+} at various ionic strengths, varying [KCl] from 0 to 200 mM. While ionic strength has no significant effect on the intradomain PREs (Fig. 3, left panels), the interdomain PREs decrease significantly as the ionic strength is increased (Fig. 3, right panels). Thus the interdomain contacts responsible for the interdomain PREs appear to be mediated by interactions that comprise a significant electrostatic component.

To discount and/or cancel out any intermolecular effects as the source of the interdomain PREs, control experiments were performed on samples comprising a mixture of $^{15}N/^{13}C/^{2}H$-labeled CaM and paramagnetically-labeled CaM at natural isotopic abundance to exclusively detect intermolecular PREs occurring under these experimental conditions. No intermolecular PREs were detected for CaM-4Ca^{2+}-MLCK or apo CaM, and only very small intermolecular PRES were observed for apo CaM in the presence of MLCK (Supplementary Fig. S5). However, some more sizeable intermolecular PREs were in fact detected for CaM-4Ca^{2+}, though still much smaller in magnitude than the intramolecular PREs. Thus, for maximal accuracy and relevance, intermolecular PRE effects were subtracted from the PREs measured for CaM-4Ca^{2+} elsewhere in this report (unless otherwise specified) to ensure that quantitative analysis was restricted to intramolecular PREs and not complicated by intermolecular effects. Interestingly, the intermolecular PREs that are observed appear to be a manifestation of the same intramolecular/interdomain interactions in CaM-4Ca^{2+} that are characterized below (Supplementary Fig. S5).

Interdomain PREs Are Unaccounted for by Current CaM Structures

Agreement between experimental PREs and those back-calculated from known structures was assessed by simulated annealing optimization of the spin-label coordinates using an ensemble representation to account for their inherent flexibility. There is excellent quantitative agreement for the intradomain PREs (Fig. 2); the intradomain PRE Q-factors (Table 1; see Eq. 1 in Methods for definition) range from 0.1 to 0.2, with the exception of those for the C-terminal domain of apo CaM (with or without bound peptide) where agreement is a little worse (Q = 0.3–0.4) owing to the presence of intermediate chemical exchange between two states within the C-terminal domain,[2,36] which causes line broadening and a concomitant decrease in the quality of the experimental PRE data. The fit of the intradomain PRE data for the C-terminal domain of apo CaM can be improved

slightly by fitting to a mixture of apo and Ca^{2+} loaded conformations at an optimal ratio of ~9:1 (Supplementary Fig. S6), in agreement with previous findings based on ^{15}N relaxation data.[36] The full PRE profiles for CaM-$4Ca^{2+}$-MLCK fit extremely well to the known X-ray structure[4] of the complex (Figs. 2*A* and *B*, top panels) with Q-factors of ~0.2 (Table 1). For the other three states of CaM, however, agreement with the interdomain PRE data is extremely poor (Figs. 2*A* and *B*, lower three panels) with Q-factors of ~1 (Table 1).

The dumbbell X-ray structure of CaM-$4Ca^{2+}$ [3,9,10] does not predict the existence of the interdomain PREs observed experimentally for CaM-$4Ca^{2+}$ or apo CaM, and indeed, a very wide range of interdomain orientations, spanning a cone of semi-angle ~90° is fully consistent with interdomain PRE values ≤ 2 s^{-1} (see below). The interdomain PRE profiles back-calculated from the structure of CaM-$4Ca^{2+}$-MLCK[4] exhibit some qualitative similarities with the experimental PRE profiles for CaM-$4Ca^{2+}$ with peaks in similar locations but yield poor quantitative fits to the experimental data (Figs. 2*A* and *B*, second row panels): in particular, the back-calculated interdomain PREs for S17C are much larger, and there are regions with both smaller (residues 34-46 and 69-80) and larger (residues 7-20) back-calculated PREs for A128C. Similar results are obtained using the crystal structure of a compact state of CaM-$4Ca^{2+}$ [11] (Fig. S4). The MD ensemble for CaM-$4Ca^{2+}$ [19] predicts some but not all features the experimental PRE profiles (Fig. S8): large intermolecular PREs are predicted for residues 47-59 from A128C where none are observed, while other experimental intermolecular PREs such as those for residues 15-19 from A128C are not predicted (Supplementary Fig. S7).

The interdomain PREs observed for apo CaM (which are qualitatively similar in the presence and absence of bound peptide) are not predicted by any of the existing structures (Figs. 2*A* and *B*, lower two panels). Moreover, the peak locations in the experimental PRE profiles of apo CaM do not coincide with those back-calculated from the structure of the CaM-$4Ca^{2+}$-MLCK complex.

Based on the above observations, one can infer, without any further analysis, that a significant fraction of the sparsely-populated compact states of CaM-$4Ca^{2+}$ samples a region of conformational space that likely overlaps with that occupied by the CaM-$4Ca^{2+}$-MLCK complex; in contrast the major fraction of sparsely-populated compact states of apo CaM (both free and bound to peptide) does not significantly overlap with the CaM-$4Ca^{2+}$-MLCK complex. Further, while the MD simulation model[19] samples compact states of CaM-$4Ca^{2+}$, the distribution and conformational space occupied by these states are not the same as those present in solution.

Visualization of Sparsely-Populated States by PRE-driven Ensemble Simulated Annealing Calculations

To obtain a quantitative description of the sparsely-populated states sampled by CaM-$4Ca^{2+}$ and apo CaM we carried out a series of PRE-driven simulated annealing calculations[29] in which the minor compact state was represented by an ensemble of varying size and population.[37] The two CaM domains were treated as rigid bodies, and only the linker residues (77-81) were given torsional degrees of freedom. The major species was represented by the extended dumbbell conformation but identical results were obtained using an ensemble generated from calculations in which the interdomain PREs were constrained to values ≤ 2 s^{-1}. From the dependence of the interdomain PRE Q-factor on ensemble size and population of the compact sparsely-populated species, it is observed that the interdomain Q-factor decreases rapidly up to a population of ~10% for CaM-$4Ca^{2+}$ and apo CaM bound to peptide (Fig. 4*A*, left and right panels), and ~5% for apo CaM without bound peptide (Fig. 4*A*, middle panel), and up to an ensemble size of 8 (Fig. 4*B*), leveling off thereafter. The apparently lower population of compact states for apo CaM is consistent

with the NMR finding that the central linker region of apo CaM appears to adopt a helical conformation about 30% of the time,[2] whereas in CaM-4Ca^{2+} there is no NMR evidence for such transient helix formation.[18] A comparison of calculated and observed intermolecular PREs yield good agreement in all cases (Figs. 4*C* and *D*; Supplementary Table S2). Note that the higher Q-factors for the interdomain PREs of apo CaM simply reflect the low magnitude of the PREs, but the rms difference between observed and calculated values is small (1.5–1.6 s^{-1}, see Table 2).

Reweighted atomic probability maps,[35] generated from the calculated ensembles and describing the spatial distribution of the compact minor states of CaM, are shown in Fig. 5. For reference, a superposition of the dumbbell extended structure of CaM-4Ca^{2+} [3] and the CaM-4Ca^{2+}-MLCK complex[4] is displayed in Fig. 5*A*, along with a probability map generated from a superposition of a large number of other peptide-bound CaM crystal structures.

We first consider the conformational space compatible with the absence of intermolecular PREs (i.e. PRE rates ≤ 2 s^{-1}) and represented by the gray probability density maps in Figs. 5*B–D*. These probability maps provide only a rough guide for the major species (population ~ 90%) for which there are no close interdomain contacts, since the calculated ensemble is defined by the absence of PREs rather than by any direct experimental measurements. In each case, the conformation of one domain relative to the other occupies roughly one full hemisphere (i.e. a cone of semi-angle ~90°). This ensemble bears a very strong resemblance in terms of size and orientation to that recently calculated on the basis of PCS, RDC and SAXS data.[17,38–40] Indeed, even the tilt of the hemisphere of the major species ensemble from the dumbbell structure is very similar in the two cases (~45° versus ~30° [17]).

The atomic probability maps describing the conformational space sampled by the compact minor states (population ≤ 10%) are plotted at multiple contour levels ranging from 0.1 (transparent blue) to 0.5 (opaque red) of maximum (Figs. 5*B–D*). While all compact state ensembles encompass a large range of conformational space, the distribution for CaM-4Ca^{2+} is clearly distinct from that of apo CaM (free or peptide-bound).

The atomic probability maps describing the conformational space sampled by the compact minor states (population ≤ 10%) are plotted at multiple contour levels ranging from 0.1 (transparent blue) to 0.5 (opaque red) of maximum (Figs. 5*B–D*). While all compact state ensembles encompass a large range of conformational space, the distribution for CaM-4Ca^{2+} is clearly distinct from that of apo CaM (free or peptide-bound).

For CaM-4Ca^{2+} about half of the compact minor species ensemble samples a region of space (Fig. 5*B*) that clearly overlaps with that occupied by the CaM-4Ca^{2+}-peptide complexes (Fig. 5*A*). We note that the atomic probability maps obtained with the S17C and A128C data are very similar to those obtained with the T5C and T117C data, or with all four PRE data sets together (Supplementary Figs. S8*B–D*). This consistency is also seen for the interdomain PRE profiles back-calculated from different ensembles obtained with various combinations of PRE data sets (Supplementary Fig. S9), providing independent validation of the results. Moreover, even calculations carried out using any of the PRE datasets individually yield similar results (Supplementary Figs. S8*E–H*). The PRE data for CaM-4Ca^{2+} provide direct and unambiguous evidence not only that the two domains of CaM-4Ca^{2+} can come into close contact in solution for a small fraction of the time (~10%), but that these compact states preferentially adopt peptide-bound-like conformations about half of the time (i.e. the population of peptide-bound-like conformations is ~5%).

Thus the PRE data presented here provide distinct, but fully complementary, information to that afforded previously by analysis of RDC, PCS and SAXS data.[17,38–40] The latter provide

direct experimental data to characterize the major species ensemble that has no interdomain contacts, but only allow an approximate estimate of the percentage (~5%) of a compact-like species that would not impact the RDC, PCS and SAXS data.[38] In this regard, it should be stressed that the contribution of close-contact minor species to the PRE is hugely enhanced relative to that of PCS owing to the $<r^{-6}>$ versus $<r^{-3}>$ dependence on the paramagnetic center-nucleus distance, and the absence of an orientational dependence of the position of the nuclear spin with respect to the principal axes of the magnetic susceptibility tensor.[21]

The atomic probability maps calculated for the sparsely-populated compact states of apo CaM in the absence (Fig. 5C) and presence (Fig 5D) of peptide are similar to one another. In contrast to CaM-4Ca^{2+}, the minor state ensemble does not cluster around the CaM-4Ca^{2+}-peptide conformations, but preferentially samples structures on the opposing interface. (Note that the accuracy of the calculated apo CaM ensembles is not as high as those for CaM-4Ca^{2+} as the magnitude interdomain PREs is smaller and the quality of the data lower due to intermediate exchange in the C-terminal domain). Thus, apo CaM samples a range of compact (5–10%) and extended (90–95%) structures, and even in the presence of peptide does not clamp down into a single compact structure as in the case of CaM-4Ca^{2+}-MLCK.

Concluding Remarks

The present findings imply that Ca^{2+} activates CaM not only through local structural changes within each domain,[2,5] but also through more global effects—with Ca^{2+} allowing CaM to clamp down upon its peptide target in a manner not possible in the apo state. This does not necessarily imply a purely conformational selection mechanism of binding, but rather that CaM-4Ca^{2+} has the predilection to form the relevant compact structures (unlike the apo state), priming it to bind peptide when present. This is fully consistent with the model proposed by Kranz et al.,[7] based on amide exchange rates, in which the initial interaction between a random coil peptide and CaM-4Ca^{2+} results in a loosely packed initial complex, followed by coil-to-helix transitions within the peptide and concomitant formation of specific intermolecular ion-pair and hydrophobic interactions to generate the final compact complex, a process akin to coupled folding and binding[41] and induced fit. CaM-4Ca^{2+} does not necessarily sample the CaM-4Ca^{2+}-MLCK structure directly (which would not be productive, since the binding surface would be largely inaccessible), but samples a range of nearby conformations, which are also near the conformations of other canonical CaM complexes (Fig. 5A), thus speaking to the universality of this process.

Earlier work has found that binding entropy varies considerably between different CaM-4Ca^{2+}-target interactions: the binding entropy is strongly correlated with differences in changes in CaM conformational entropy upon binding, which arise from highly localized sub-nanosecond side chain motions.[42,43] In contrast, here we examine large-scale rigid-body domain motions in CaM; given the conserved overall conformation of CaM-4Ca^{2+}-target complexes (Fig. 5A), the decrease in conformational entropy due to the loss of these motions upon binding would not be expected to vary considerably between interactions with different targets.

The salt dependence of the interdomain PREs in CaM-4Ca^{2+} (Fig. 3) indicates that the formation of these compact structures is at least partially driven by electrostatic forces. The surface potential of apo CaM is dominated by large areas of negative charge (Supplementary Fig S10A–D). CaM-4Ca^{2+} is similarly negatively charged; however, additional positively charged patches are present on its surface as a result of the charge of the four Ca^{2+} ions and the structural rearrangements they induce (Supplementary Fig. S10E–H). One of these positively charged patches partially overlaps with the interdomain interaction site (Fig. 5B) on the N-terminal domain, while the interaction site on the C-terminal domain remains highly negatively charged. Such interactions would be much less favorable in apo CaM due

to electrostatic repulsion. The role of electrostatic contacts in protein-protein encounter complex formation has also been observed in other systems.[37,44]

The PRE data also imply an alternative pathway of CaM action; instead of the scheme illustrated in Figs. 1*A*–*C* where CaM remains unbound until activated by Ca^{2+}, CaM could remain associated with its kinase targets (via its C-terminal domain) even in the resting state, and then only activate the kinase when Ca^{2+} loading causes it to clamp down upon the CBD, thus relieving kinase self-inhibition. CaM is known to bind to some of its non-canonical targets in a Ca^{2+}-independent manner[1], and weak interactions between apo CaM and MLCK peptides have been reported[45,46]. Although the CBD of the kinase remains self-associated in the resting state,[47] the portion that interacts with the C-terminal domain of CaM is partially exposed, potentially allowing the CaM C-terminal domain to bind without causing activation (Supplementary Fig. S11). Such a model would make activation dependent on Ca^{2+} loading in the N-terminal domain, which is reasonable, as the C-terminal domain is likely to be partially Ca^{2+}-loaded even at the resting intracellular Ca^{2+} concentration of ~100 nM due to its much higher Ca^{2+} affinity.[48] Whether the C-terminal domain of apo CaM remains associated with its peptide targets or just interacts with them transiently, this is compatible with the idea that target binding and activation by CaM is initiated by the C-terminal domain,[49] with the N-terminal domain then acting as the primary Ca^{2+} sensor. [50]

The current PRE data on CaM, in conjunction with previously published PRE data that revealed the existence of an open-to-partially closed transition for apo maltose binding protein,[51] also suggest an alternative perspective on conformational selection and induced fit for proteins where ligand binding results in interdomain reorientations that effectively trap the ligand and bury it from solvent. In such systems, it is evident that the holo conformation cannot itself bind ligand directly, since the ligand-binding site is not accessible. However, the existence of sparsely-populated states that are partially closed yet still accessible to ligand, and that occupy a region of conformational space in reasonably close proximity to that of the holo state, may facilitate the transition to the closed ligand-bound complex, highlighting the complementarity and interplay of conformational selection and induced fit.

Supplementary Material

Refer to Web version on PubMed Central for supplementary material.

Acknowledgments

References

1. Yamniuk AP, Vogel HJ. Mol Biotechnol. 2004; 27:33–57. [PubMed: 15122046]

2. Kuboniwa H, Tjandra N, Grzesiek S, Ren H, Klee CB, Bax A. Nature Struct Biol. 1995; 2:768–776. [PubMed: 7552748]

3. Chattopadhyaya R, Meador WE, Means AR, Quiocho FA. J Mol Biol. 1992; 228:1177–1192. [PubMed: 1474585]

4. Meador WE, Means AR, Quiocho FA. Science. 1992; 257:1251–1255. [PubMed: 1519061]

5. Zhang M, Tanaka T, Ikura M. Nature Struct Biol. 1995; 2:758–767. [PubMed: 7552747]

6. Ikura M, Clore GM, Gronenborn AM, Zhu G, Klee CB, Bax A. Science. 1992; 256:632–638. [PubMed: 1585175]

7. Kranz JK, Flynn PF, Fuentes EJ, Wand AJ. Biochemistry. 2002; 41:2599–2608. [PubMed: 11851407]

8. Hoeflich KP, Ikura M. Cell. 2002; 108:739–42. [PubMed: 11955428]

9. Babu YS, Sack JS, Greenhough TJ, Bugg CE, Means AR, Cook WJ. Nature. 1985; 315:37–40. [PubMed: 3990807]

10. Wilson MA, Brunger AT. J Mol Biol. 2000; 301:1237–1256. [PubMed: 10966818]

11. Fallon JL, Quiocho FA. Structure. 2003; 11:1303–1307. [PubMed: 14527397]

12. Slaughter BD, Bieber-Urbauer RJ, Johnson CK. J Phys Chem B. 2005; 109:12658–12662. [PubMed: 16852567]

13. Trewhella J. Cell Calcium. 1992; 13:377–90. [PubMed: 1505003]

14. Tjandra N, Kuboniwa H, Ren H, Bax A. Eur J Biochem. 1995; 230:1014–1024. [PubMed: 7601131]

15. Barbato G, Ikura M, Kay LE, Pastor RW, Bax A. Biochemistry. 1992; 31:5269–5278. [PubMed: 1606151]

16. Baber JL, Szabo A, Tjandra N. J Am Chem Soc. 2001; 123:3953–3959. [PubMed: 11457145]

17. Bertini I, Del Bianco C, Gelis I, Katsaros N, Luchinat C, Parigi G, Peana M, Provenzani A, Zoroddu MA. Proc Natl Acad Sci U S A. 2004; 101:6841–6846. [PubMed: 15100408]

18. Chou JJ, Li S, Klee CB, Bax A. Nature Struct Biol. 2001; 8:990–997. [PubMed: 11685248]

19. Gsponer J, Christodoulou J, Cavalli A, Bui JM, Richter B, Dobson CM, Vendruscolo M. Structure. 2008; 16:736–746. [PubMed: 18462678]

20. Iwahara J, Clore GM. Nature. 2006; 440:1227–1230. [PubMed: 16642002]

21. Clore GM, Iwahara J. Chem Rev. 2009; 109:4108–4139. [PubMed: 19522502]

22. Clore GM, Gronenborn AM. Meth Enzymol. 1994; 239:349–363. [PubMed: 7830590]

23. Delaglio F, Grzesiek S, Vuister GW, Zhu G, Pfeifer J, Bax A. J Biomol NMR. 1995; 6:277–293. [PubMed: 8520220]

24. Hu K, Doucleff M, Clore GM. J Magn Reson. 2009; 200:173–177. [PubMed: 19615926]

25. Iwahara J, Tang C, Marius Clore G. J Magn Reson. 2007; 184:185–195. [PubMed: 17084097]

26. Mulder FA, Schipper D, Bott R, Boelens R. J Mol Biol. 1999; 292:111–123. [PubMed: 10493861]

27. Ulrich EL, Akutsu H, Doreleijers JF, Harano Y, Ioannidis YE, Lin J, Livny M, Mading S, Maziuk D, Miller Z, Nakatani E, Schulte CF, Tolmie DE, Kent Wenger R, Yao H, Markley JL. Nucl Acids Res. 2008; 36:D402–D408. [PubMed: 17984079]

28. Schwieters CD, Kuszewski JJ, Tjandra N, Clore GM. J Magn Reson. 2003; 160:65–73. [PubMed: 12565051]

29. Schwieters CD, Kuszewski JJ, Clore GM. Progr Nucl Magn Reson Spec. 2006; 48:47–62.

30. Iwahara J, Schwieters CD, Clore GM. J Am Chem Soc. 2004; 126:5879–5896. [PubMed: 15125681]

31. Clore GM, Kiuszewski J. J Am Chem Soc. 2002; 124:2866–2867. [PubMed: 11902865]

32. Chang SL, Szabo A, Tjandra N. J Am Chem Soc. 2003; 125:11379–11384. [PubMed: 16220961]

33. Clore GM, Schwieters CD. J Am Chem Soc. 2004; 126:2923–2938. [PubMed: 14995210]

34. Schwieters CD, Clore GM. J Magn Reson. 2001; 152:288–302. [PubMed: 11567582]

35. Schwieters CD, Clore GM. J Biomol NMR. 2002; 23:221–225. [PubMed: 12238594]

36. Malmendal A, Evenas J, Forsen S, Akke M. J Mol Biol. 1999; 293:883–899. [PubMed: 10543974]

37. Tang C, Iwahara J, Clore GM. Nature. 2006; 444:383–386. [PubMed: 17051159]

38. Bertini I, Giachetti A, Luchinat C, Parigi G, Petoukhov MV, Pierattelli R, Ravera E, Svergun DI. J Am Chem Soc. 2010; 132:13553–13558. [PubMed: 20822180]

39. Bertini I, Gupta YK, Luchinat C, Parigi G, Peana M, Sgheri L, Yuan J. J Am Chem Soc. 2007; 129:12786–94. [PubMed: 17910448]

40. Dasgupta S, Hu X, Keizers PH, Liu WM, Luchinat C, Nagulapalli M, Overhand M, Parigi G, Sgheri L, Ubbink M. J Biomol NMR. 2011 epub ahead of print. 10.1007/s10858-011-9532-2

41. Sugase K, Dyson HJ, Wright PE. Nature. 2007; 447:1021–5. [PubMed: 17522630]

42. Marlow MS, Dogan J, Frederick KK, Valentine KG, Wand AJ. Nat Chem Biol. 2010; 6:352–8. [PubMed: 20383153]

43. Frederick KK, Marlow MS, Valentine KG, Wand AJ. Nature. 2007; 448:325–9. [PubMed: 17637663]

44. (a) Volkov AN, Worrall JA, Holtzmann E, Ubbink M. Proc Natl Acad Sci U S A. 2006; 103:18945–50. [PubMed: 17146057] (b) Suh J-Y, Tang C, Clore GM. J Am Chem Soc. 2007; 129:12954–12955. [PubMed: 17918946]

45. Klevit RE, Blumenthal DK, Wemmer DE, Krebs EG. Biochemistry. 1985; 24:8152–7. [PubMed: 3841496]

46. Tsvetkov PO, Protasevich, Gilli R, Lafitte D, Lobachov VM, Haiech J, Briand C, Makarov AA. J Biol Chem. 1999; 274:18161–4. [PubMed: 10373414]

47. Goldberg J, Nairn AC, Kuriyan J. Cell. 1996; 84:875–887. [PubMed: 8601311]

48. Gilli R, Lafitte D, Lopez C, Kilhoffer M, Makarov A, Briand C, Haiech J. Biochemistry. 1998; 37:5450–5456. [PubMed: 9548926]

49. Bayley PM, Findlay WA, Martin SR. Protein Sci. 1996; 5:1215–28. [PubMed: 8819155]

50. Rodriguez-Castaneda F, Maestre-Martinez M, Coudevylle N, Dimova K, Junge H, Lipstein N, Lee D, Becker S, Brose N, Jahn O, Carlomagno T, Griesinger C. EMBO J. 2010; 29:680–91. [PubMed: 20010694]

51. Tang C, Schwieters CD, Clore GM. Nature. 2007; 449:1078–1082. [PubMed: 17960247]

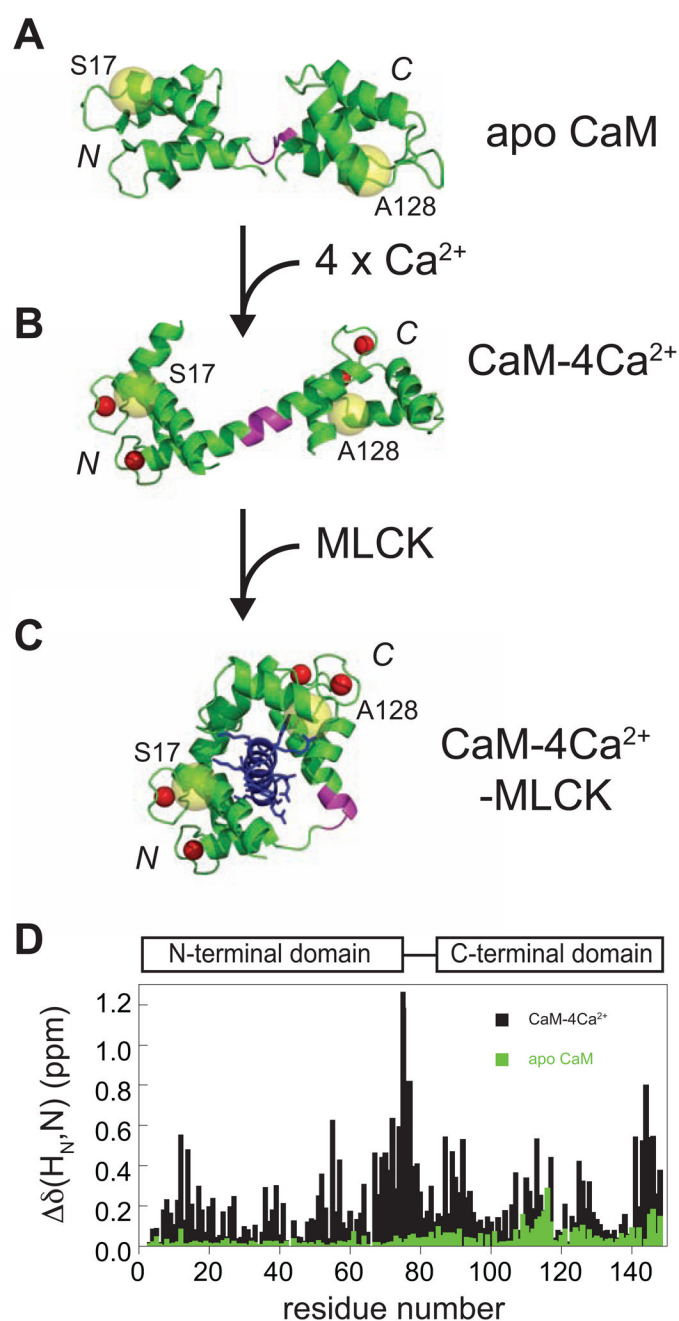**Fig. 1. CaM structures and peptide interactions**

(*A–C*) Structures of CaM in various physiological states. Ca^{2+} ions are shown as red spheres, and spin-labeling sites S17C and A128C are indicated by yellow spheres. The flexible linker (residues 77-81)[15] is shown in magenta. (*A*) NMR structure of apo CaM (PDB 1CFD).[2] (*B*) Crystal structure of CaM-4Ca^{2+} (PDB 1CLL)[3] in the extended dumbbell conformation with a continuous central helix. (*C*) Crystal structure of the CaM-4Ca^{2+}-MLCK complex (PDB 1CDL).[4] (*D*) Weighted combined $^1H_N/^{15}N$ chemical shift perturbations, $\Delta\delta(H_N,N)$, for the backbone amide groups of apo CaM (green) or CaM-4Ca^{2+} (black) upon saturation with MLCK peptide.
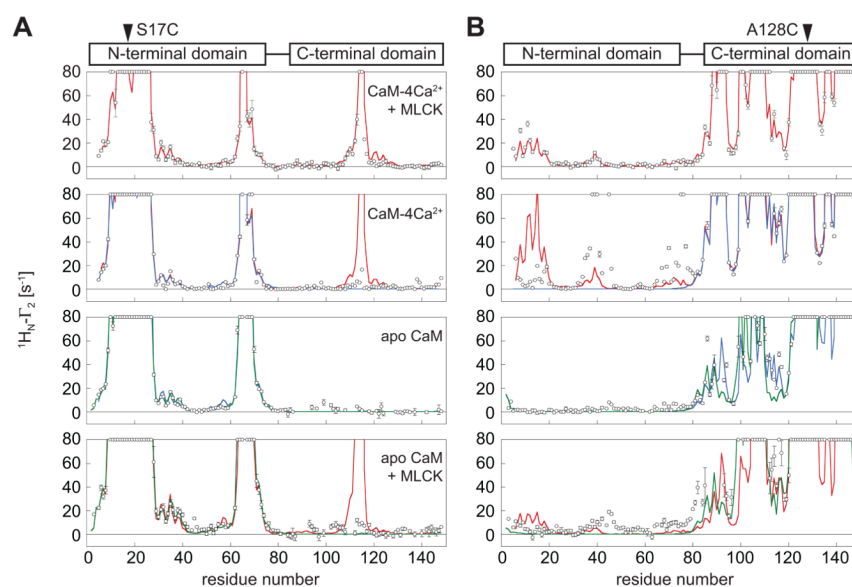
Fig. 2. PRE profiles

(*A,B*) PRE profiles for CaM with a spin-label at (*A*) S17C or (*B*) A128C. Experimental PRE profiles for apo or Ca^{2+}-loaded CaM, in the presence or absence of MLCK peptide, are shown as circles (error bar, 1 s.d.). PREs too large (> 80 s^{-1}, roughly) to be accurately measured are plotted at the top of the charts. PRE profiles back-calculated from the structures of CaM-4Ca^{2+}-MLCK (red), CaM-4Ca^{2+} (blue) and apo CaM (green) are shown as solid lines. Only for the CaM-4Ca^{2+}-MLCK complex are the experimental interdomain PREs correctly predicted by the corresponding known structure. Note that slightly different PRE profiles can be back-calculated from the same structure depending on which experimental intradomain PRE data set is used to fit the spin-label position (and, in the case of CaM-4Ca^{2+}-MLCK, whether the peptide is present—as in the top panel—which slightly restricts the conformational space available to the spin-label). In the case of A128C, the apo NMR structure predicts some small PREs at the N-terminus; these are likely artifacts of the specific conformation adopted by the deposited average regularized structure (PDB 1CFD) since no interdomain NOEs were observed in that study.[2]
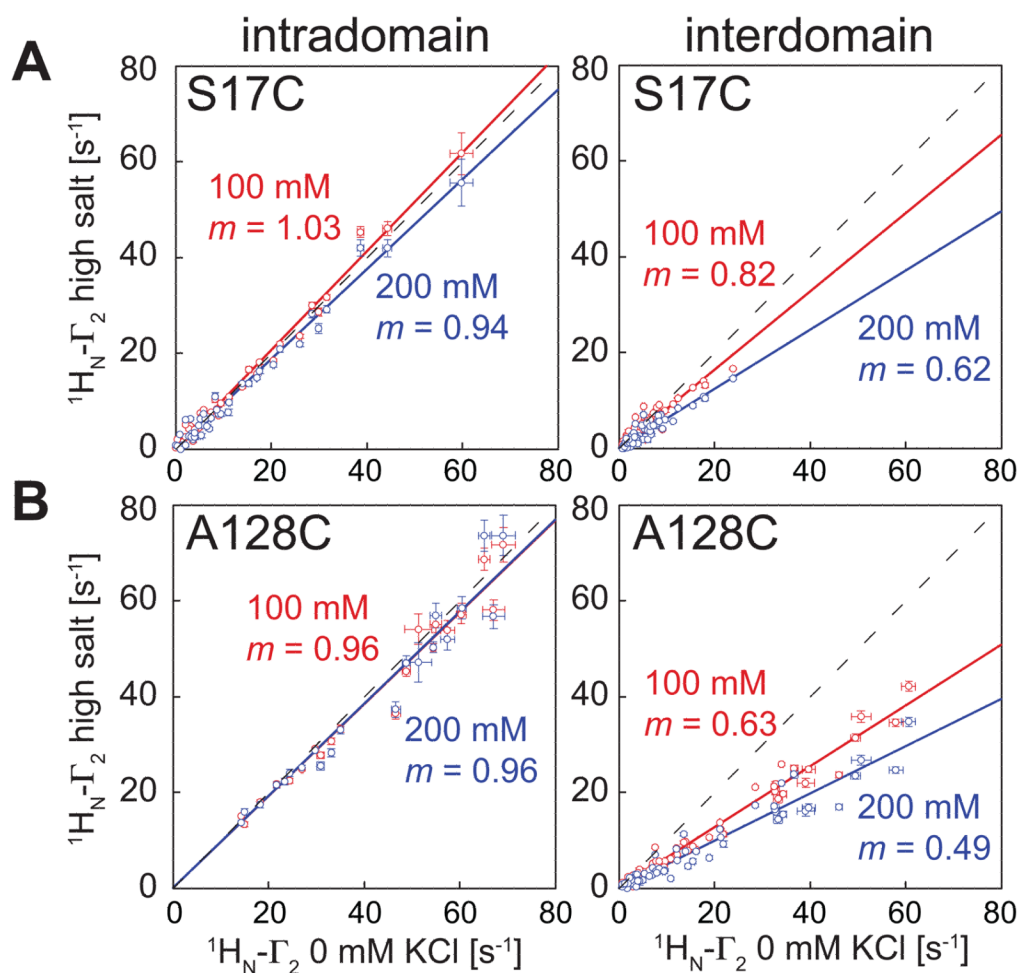
Fig. 3. Ionic strength dependence of CaM-Ca^{2+} PREs

Experimental PREs (circles, error bars = 1 s.d.) were measured for CaM-4Ca^{2+} with the nitroxide spin label at (*A*) S17C and (*B*) A128C at various ionic strengths. Intradomain PREs are shown in the left panels and interdomain PREs in the right panels. The data are presented as scatter plots with the PRE value at 0 mM KCl shown on the *x*-axis and the PRE value at 100 mM (red) and 200 mM (blue) shown on the *y*-axis. In each case, the slope of a best-fit line through the origin is given. A dashed line corresponding to a slope of *m* = 1 is also displayed for reference. The intradomain PREs do not depend on ionic strength, but increasing the salt concentration significantly decreases the magnitude of the interdomain PREs, indicating that the interdomain interactions explored have a significant electrostatic component.
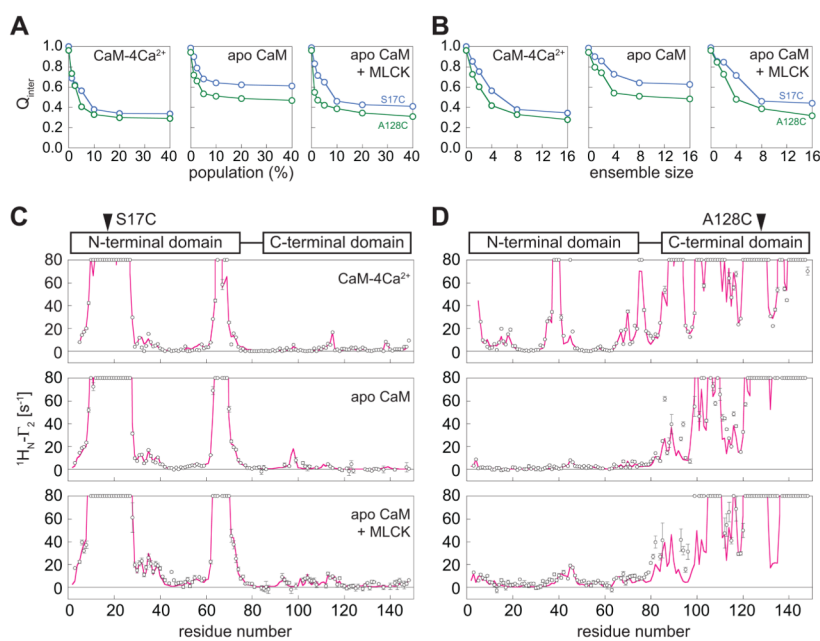
Fig. 4. PRE-driven ensemble simulated annealing calculations characterizing the minor closed states of CaM with interdomain contacts

(*A,B*) Dependence of the interdomain PRE Q-factor for S17C (blue) and A128C (green) as a function of (*A*) minor state population (using an 8-member ensemble) and (*B*) ensemble size (for a minor state population of 10%) for CaM-4Ca^{2+}, apo CaM, and apo CaM + MLCK peptide. (*C,D*) The resulting fits to the PRE profiles for (*C*) S17C and (*D*) A128C for a minor state population of 10% represented by an 8-member ensemble (calculated, magenta lines; experimental, black circles; error bars, 1 s.d.).
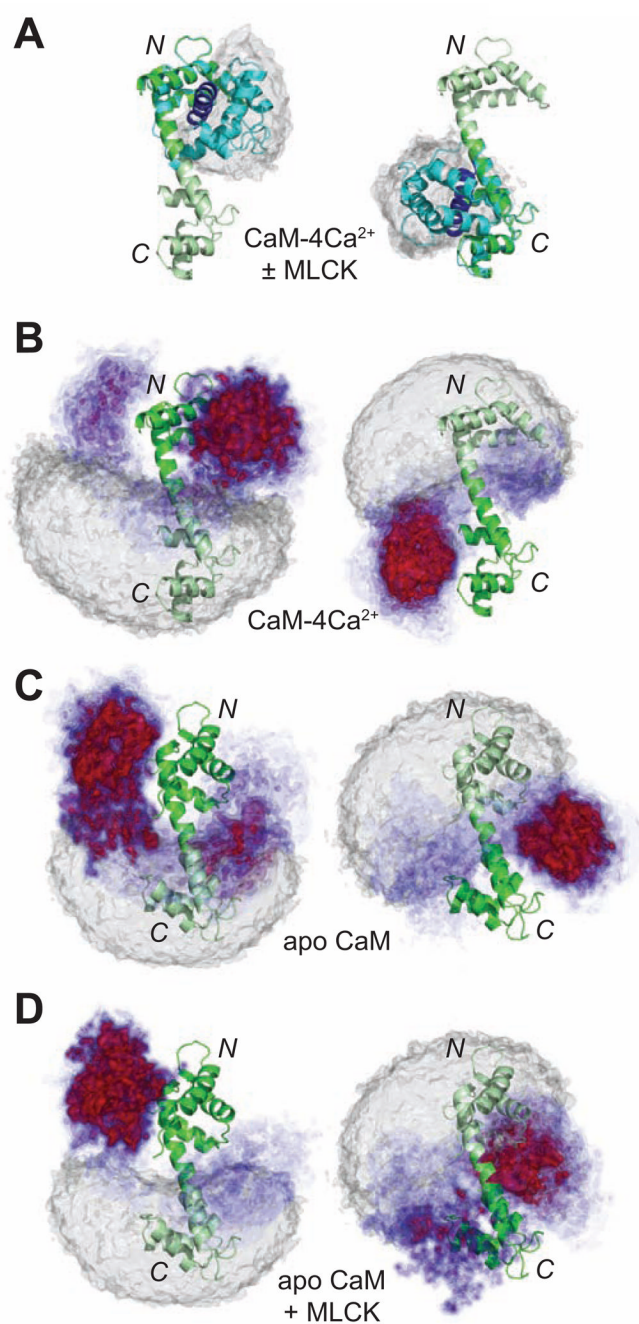
Fig. 5. Visualizing the minor closed-state ensembles of CaM-4Ca^{2+} and apo CaM
(*A*) CaM-4Ca^{2+}-MLCK complex[4] (with CaM in cyan and MLCK peptide in blue) overlaid on the CaM-4Ca^{2+} dumbbell structure[3] (green), best-fitted to either the N-terminal (left panel) or C-terminal (right panel) domains. Twenty-six additional peptide-bound structures were overlaid in the same manner, and these are represented by the atomic probability density maps[35] shown in grey for the C-terminal domain (left) and N-terminal domain (right). These structures (PDB codes 1CDL, 1CDM, 1MXE, 1NIW, 1QS7, 1QTX, 1VRK, 1YR5, 1ZUZ, 2BE6, 2F3Y, 2F3Z, 2FOT, 2HQW, 2O5G, 2O60, 2VAY, 3BXL, 3BYA, 3DVE, 3DVJ, 3DVK, 3DVM, 3EWT, 3EWV, 3GP2) represent a wide array of different 1:1 canonical CaM-peptide complexes, but it can be seen that the conformational space

occupied by the two domains is very similar to that in the CaM-4Ca^{2+}-MLCK complex. (*B*–*D*) Atomic probability density maps showing the conformational space sampled by the minor species ensemble for (*B*) CaM-4Ca^{2+}, (*C*) apo CaM, and (*D*) the apo CaM-MLCK complex. The minor state atomic probability maps are derived from 100 independent PRE-driven simulated annealing calculations using an 8-member ensemble (i.e. 800 total structures) at a population of 10%, and plotted at multiple contour levels ranging from 0.1 (transparent blue) to 0.5 (opaque red). The gray probability density maps, plotted at a single contour level of 0.1 of maximum, show the conformational space consistent with interdomain PRE values ≤ 2 s^{-1} and represent the major state ensemble characterized by no interdomain contacts and an occupancy of ~90% (see also Fig. S9*A*). In the left-hand panels, all ensemble members are best-fitted to the N-terminal domain (dark green) and the probability density maps are shown for the C-terminal domain. In the right-hand panels, all ensembles are best-fitted to the C-terminal domain (dark green) and the probability density maps are shown for the N-terminal domain. All panels are displayed in the same orientation, and the extended dumbbell structure[3] is displayed as a ribbon diagram for reference (with the structures of the individual domains in panels *C* and *D* replaced by those for apo CaM).

Table 1

Q-factors for fits of CaM PRE data

	intradomain fit[a]			full molecule fit[b]		
	intra	inter	all	intra	inter	all
CaM-4Ca²⁺-MLCK[c]						
S17C	0.16	0.41	0.22	0.17	0.21	0.18
A128C	0.13	0.34	0.17	0.13	0.25	0.15
CaM-4Ca²⁺ [d]						
S17C	0.17	0.99	0.29	0.17	0.99	0.29
A128C	0.13	0.99	0.49	0.14	0.99	0.49
Apo CaM[e]						
S17C	0.16	0.96	0.17	0.16	0.96	0.17
A128C	0.35	0.93	0.36	0.35	0.93	0.36
Apo CaM + MLCK[e]						
S17C	0.20	0.96	0.30	0.20	0.96	0.30
A128C	0.42	0.93	0.55	0.44	0.92	0.54

[a]Paramagnetic tag positions were fit to intradomain PREs only (residues 1-76 for the N-terminal domain; residues 83-148 for the C-terminal domain), and the Q-factors were then calculated for intradomain, interdomain, or all PREs.

[b]Paramagnetic tag positions were fit to PREs for the full molecule, and Q-factors were then calculated for intradomain, interdomain, or all PREs.

[c]Q-factors calculated for experimental PREs from CaM-4Ca²⁺-MLCK, fit to crystal structure of CaM-4Ca²⁺-MLCK complex (PDB 1CDL)[4] (Fig. 1C).

[d]Q-factors calculated for experimental PREs from CaM-4Ca²⁺, fit to "dumbbell" crystal structure of CaM-4Ca²⁺ (PDB 1CLL)[3] (Fig. 1B).

[e]Q-factors calculated for experimental PREs from Ca²⁺-free CaM (with or without peptide, as indicated), fit to NMR structure of apo CaM (PDB 1CFD)[2] (Fig. 1A). Note that while the structure for the entire molecule of apo CaM was deposited in the PDB and is used in the calculations presented in this table, there were, in fact, no interdomain NOE restraints (or any other NMR restraints) to orient the two domains relative to one another.[2]

Table 2

Goodness of fit for interdomain PRE data with and without minor states generated by simulated annealing calculations

	Q-factor		rms difference (s^{-1})	
	major alone[a]	major + minor[b]	major alone[a]	major + minor[b]
CaM-4Ca^{2+}				
S17C	0.99	0.38	3.1	1.2
A128C	0.96	0.33	12.7	4.3
Apo CaM				
S17C	0.99	0.64	2.4	1.6
A128C	0.94	0.51	2.8	1.5
Apo CaM + MLCK				
S17C	0.99	0.46	4.7	2.2
A128C	0.96	0.39	7.9	3.2

[a] Paramagnetic tag positions were first fit to the intradomain PRE data (residues 1-76 for N-terminal domain, 83-148 for C-terminal domain), and then the PRE Q-factors and rms differences between observed and calculated PREs were determined for the interdomain PREs using the extended dumbbell crystal structure (1CLL)[3] for CaM-4Ca^{2+}. Note that a very wide-range of interdomain orientations spanning a cone of semi-angle ~90° (cf. gray atomic probability density maps in Fig. 5*B*–*D* and in Supplementary Fig. S8*A*) is fully consistent with interdomain PRE values $\leq 2s^{-1}$ and yields the same results as the extended dumbbell crystal structure. Thus, the major state comprises all states with no interdomain contacts.

[b] Paramagnetic spin-label positions were first fit to intradomain PREs. PRE-driven ensemble simulated annealing calculations were then performed with an 8-member minor state ensemble encompassing 10% of the total population giving the linker region (residues 77-81) torsional degrees of freedom. Interdomain Q-factors and rms differences between observed and calculated PREs were then determined for the entire ensemble.